

Flow4D: Leveraging 4D Voxel Network for LiDAR Scene Flow Estimation

Jaeyeul Kim¹, Jungwan Woo¹, Ukcheol Shin², Jean Oh², and Sunghoon Im¹

Abstract—Understanding the motion states of the surrounding environment is critical for safe autonomous driving. These motion states can be accurately derived from scene flow, which captures the three-dimensional motion field of points. Existing LiDAR scene flow methods extract spatial features from each point cloud and then fuse them channel-wise, resulting in the implicit extraction of spatio-temporal features. Furthermore, they utilize 2D Bird’s Eye View and process only two frames, missing crucial spatial information along the Z-axis and the broader temporal context, leading to suboptimal performance. To address these limitations, we propose Flow4D, which temporally fuses multiple point clouds after the 3D intra-voxel feature encoder, enabling more explicit extraction of spatio-temporal features through a 4D voxel network. However, while using 4D convolution improves performance, it significantly increases the computational load. For further efficiency, we introduce the Spatio-Temporal Decomposition Block (STDB), which combines 3D and 1D convolutions instead of using heavy 4D convolution. In addition, Flow4D further improves performance by using five frames to take advantage of richer temporal information. As a result, the proposed method achieves a 45.9% higher performance compared to the state-of-the-art while running in real-time, and won 1st place in the 2024 Argoverse 2 Scene Flow Challenge. The code is available at <https://github.com/dgist-cvlab/Flow4D>.

Index Terms—Autonomous driving, LiDAR, scene flow

I. INTRODUCTION

LIDAR provides accurate 3D distance measurements, making it widely used in autonomous vehicles (AVs). Given its precision and reliability, extensive research on LiDAR-based detection and semantic segmentation [1], [2] has been conducted to perceive the static states of the environment. These static states, such as the positions and sizes of objects and the semantic information of the surroundings, are crucial for understanding the driving environment. However, for safe autonomous driving, information about the motion of surrounding objects is also essential. Understanding these dynamic states allows AVs to avoid potential collisions and navigate more safely. Due to this importance, LiDAR-based scene flow is emerging as a major topic in autonomous driving.

LiDAR-based scene flow studies aim to provide a detailed motion representation of the surrounding environment by estimating the 3D flow vector of each point. Numerous self-supervised methods [5], [6], [7], [8], [9] that do not require human-annotated data have been proposed, but they have not provided satisfactory performance. In contrast, supervised

(Corresponding author: Sunghoon Im.)

¹Jaeyeul Kim, Jungwan Woo, and Sunghoon Im are with the Department of Electrical Engineering and Computer Science, DGIST, Daegu, 42988, Republic of Korea (email: {jykim94, friendship1, sunghoonim}@dgist.ac.kr)

²U. Shin and J. Oh are with Robotics Institute, Carnegie Mellon University, Pittsburgh, Pennsylvania, 15217, United States {ushin, hyaejinoh}@andrew.cmu.edu

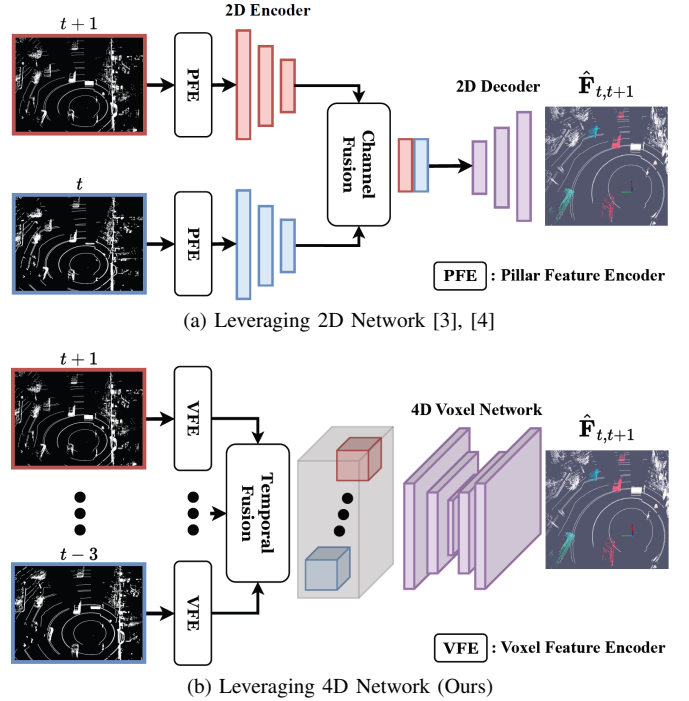


Fig. 1. Fusion strategy comparison for LiDAR scene flow estimation. (a) Existing methods [3], [4] use a 2D pillar representation and find correspondences via channel fusion followed by a 2D decoder. However, these methods only allow limited channel-level interaction due to their 2D representation. (b) In contrast, our proposed method allows explicit spatio-temporal interaction to find accurate correspondences by using a 4D voxel representation.

methods [4], [10] show improved results, thanks to the large-scale Argoverse 2 [11] scene flow dataset. However, most supervised methods also suffer from suboptimal performance because they fail to explicitly extract spatio-temporal features. This is because they first extract spatial features from each point cloud and then fuse them channel-wise to obtain temporal correlations, as shown in Fig. 1-(a). In addition, they use only two frames, missing the richer temporal context available in additional past frames.

To overcome these limitations, we propose Flow4D, a straightforward and highly effective LiDAR-based scene flow framework that temporally fuses point clouds and uses a 4D voxel network to explicitly extract spatio-temporal features. We first 3D voxelize each point cloud with a simple intra-voxel feature encoder (VFE). After that, by adding a time dimension to each 3D voxel and then concatenating along this new axis to form a 4D voxel space, the spatio-temporal features can be directly extracted. While 4D convolution can explicitly extract spatial and temporal features simultaneously, it is computa-

tionally intensive. To solve this issue, we propose the Spatio-Temporal Decomposition Block (STDB), which separates 4D convolution into 3D spatial and 1D temporal convolutions, enabling more efficient computation. Additionally, owing to its early fusion design that fuses point clouds immediately after the VFE, our method can efficiently utilize more point clouds, leveraging their richer temporal information. As a result, our Flow4D achieves superior performance compared to existing state-of-the-art methods while maintaining high computational efficiency that allows for real-time operation.

Our contributions can be summarized as follows:

- We present Flow4D, a simple yet highly effective 4D voxel-based scene flow framework that explicitly extracts spatio-temporal information from multiple point clouds.
- We introduce the Spatio-Temporal Decomposition Block (STDB), which enhances computational efficiency by decomposing 4D convolution into 3D spatial and 1D temporal convolutions.
- The proposed method outperforms the existing state-of-the-art by 45.9% on the Argoverse 2 dataset, running at a real-time speed of 15.1 FPS on an RTX 3090 GPU.

II. RELATED WORK

A. LiDAR Data Processing

LiDAR point clouds are unordered, unstructured, and irregular, making the direct application of convolution operations difficult. Therefore, to process point clouds, three methods are typically used: projection-based, point-based, and voxel-based approaches. Firstly, projection-based methods convert 3D point clouds into a 2D grid form, such as Bird's Eye View (BEV) [12], [1] or Range View (RV) [13], [14]. These methods have the advantage of efficiently compressing 3D data into 2D data. However, BEV may lose detailed information on the z-axis and RV suffer from distortion of receptive field. Secondly, point-based methods [15], [16] directly extract features from raw point clouds, thus avoiding data distortion issues. However, their computational efficiency can be a bit lower when applied to large-scale 3D data. Lastly, voxel-based methods [17], [18] convert point clouds into a regular grid of voxels, enabling the use of efficient 3D or 4D convolution operations. Combined with sparse convolutions [19], [20], voxel-based methods can efficiently operate while preserving geometric information.

B. LiDAR-based Self-supervised Scene Flow Estimation

Labeling point-wise scene flow in 3D LiDAR point clouds is very costly, which has led to the development of various self-supervised studies [21], [22], [23], [5], [24], [6], [7], [8], [9], [25]. Li et al. [5] propose a method that uses a neural scene flow prior to regularize the scene flow problem by leveraging runtime optimization, enabling better generalization to new environments. FastNSF [6] replaces the computationally expensive Chamfer loss with a distance transform-based loss in a runtime optimization-based neural scene flow pipeline. Liu et al. [7] present a self-supervised multi-frame scene flow estimation method that leverages temporal information from previous point cloud frames to enhance accuracy and

generalization performance. ZeroFlow [8] leverages label-free optimization [5] to generate pseudo-labels, supervising feedforward model [3] without human annotations. This approach combines the efficiency of feedforward method with the robustness of optimization technique, enabling scalable and fast scene flow estimation. Lin et al. [9] propose ICP-Flow, a learning-free scene flow estimator that leverages the Iterative Closest Point (ICP) algorithm with a histogram-based initialization. SeFlow [25] employs DUFOMap to classify point clouds into dynamic and static points and utilizes HDBSCAN to cluster the dynamic points. However, as large-scale human-annotated datasets have emerged, these self-supervised studies face the limitation of inferior performance compared to the latest supervised methods.

C. LiDAR-based Supervised Scene Flow Estimation

With the advent of the human-annotated scene flow datasets, various supervised scene flow methods [26], [27], [28], [29], [30], [31], [3], [32], [4], [10] have emerged. Jund et al. [3] introduce FastFlow3D, an efficient approach that converts 3D point clouds into a 2D Bird's Eye View (BEV) using pillar encoding [12]. They employ a U-Net style 2D network to enable real-time flow estimation even with large-scale LiDAR data. DeFlow [4] addresses the loss of point-wise features during the voxelization process by refining voxel features and point features through a Gated Recurrent Unit. Additionally, they propose a novel loss function that dynamically adjusts weights based on the motion states of each point. Khatri et al. [10] point out that traditional metrics fail to properly reflect the performance on small objects. They propose a new class-aware and speed-normalized metric called Bucket Normalized Endpoint Error (EPE). Additionally, they introduce TrackFlow, which uses a class-aware off-the-shelf detector and a 3D Kalman filter to estimate 3D scene flow. While previous methods [3], [4], [10] use only two point clouds, extracting spatial features from each and obtaining correlations through a decoder or Kalman filter, our Flow4D simultaneously extracts spatial and temporal features from multiple point clouds using a 4D voxel network.

III. PROPOSED METHOD

In this section, we present Flow4D, a 4D voxel-based scene flow framework, with an overview provided in Fig. 2. First, in Section III-A, we provide a brief overview of the 3D scene flow task. In Section III-B, we introduce a method for creating 4D voxel representations by temporally fusing sequential point clouds. Section III-C and Section III-D explain the 4D voxel network and the point head, respectively.

A. LiDAR-based Scene Flow

3D scene flow task aims to estimate the flow vector $\mathbf{F}_{t,t+1} \in \mathbb{R}^{N_t \times 3}$ from the current point cloud $\mathbf{P}_t \in \mathbb{R}^{N_t \times 3}$ to the next time step point cloud $\mathbf{P}_{t+1} \in \mathbb{R}^{N_{t+1} \times 3}$, where N_t represents the number of points at time step t . The scene flow vector $\mathbf{F}_{t,t+1}$ can be decomposed into the ego-vehicle's motion and the motion vector of individual points, as follows:

$$\mathbf{F}_{t,t+1} = \mathbf{F}_{t,t+1}^{\text{ego}} + \mathbf{F}_{t,t+1}^{\text{motion}}. \quad (1)$$

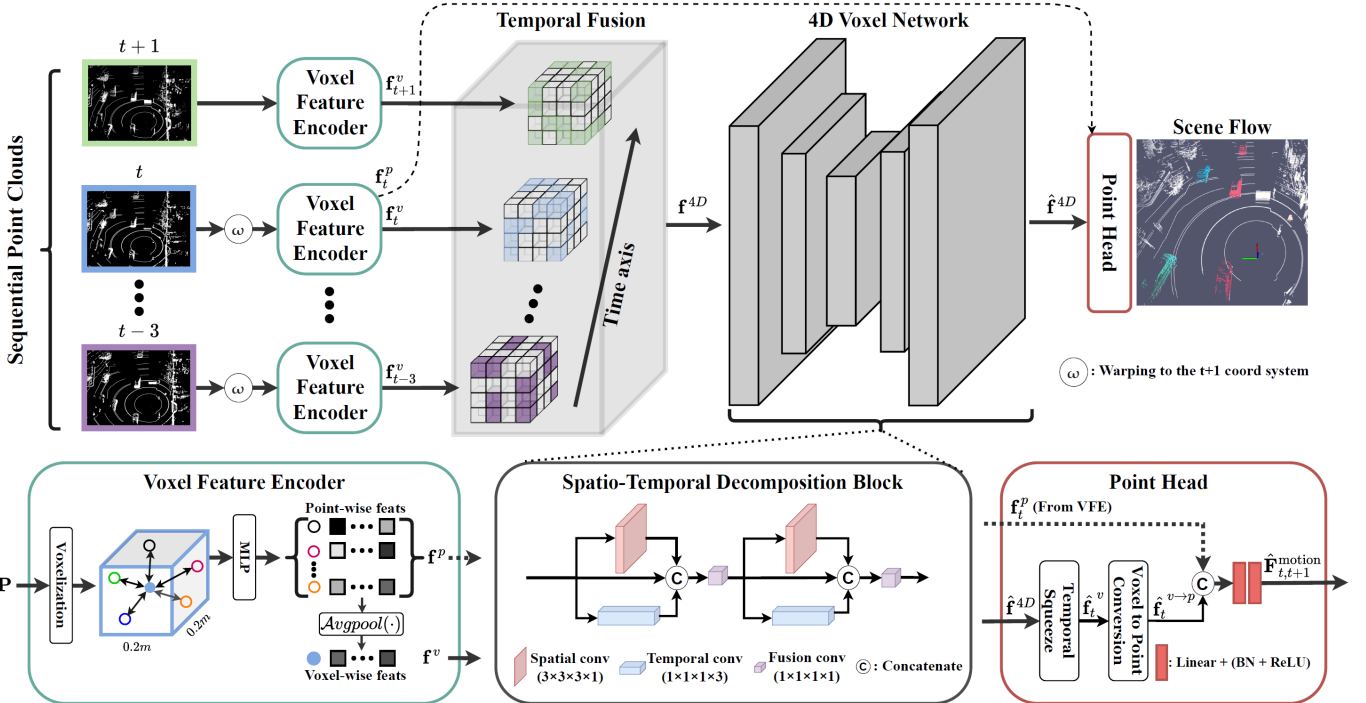


Fig. 2. Overall framework of the Flow4D. Sequential point clouds are processed through individual Voxel Feature Encoders to extract intra-voxel features. These features are then temporally fused to form 4D voxel features. The 4D voxel network, which consists of Spatio-Temporal Decomposition Blocks (STDBs), extracts voxel-wise spatio-temporal features. Finally, the Point Head module estimates point-wise flow vectors.

Following previous studies [3], [4], [8], [10], we assume that $\mathbf{F}_{t,t+1}^{\text{ego}}$ is given and aim to obtain $\mathbf{F}_{t,t+1}^{\text{motion}}$.

B. Temporal Fusion

Existing studies predict motion vectors $\hat{\mathbf{F}}_{t,t+1}^{\text{motion}}$ using only \mathbf{P}_t and \mathbf{P}_{t+1} , but we find that leveraging additional past point clouds provides richer temporal cues to improve the accuracy of current flow prediction. In this paper, we use five consecutive point clouds \mathbf{P}_τ from the time steps τ :

$$\tau \in \{t-3, t-2, t-1, t, t+1\}. \quad (2)$$

First, following previous studies [3], [4], we warp all point clouds to the coordinate system at $t+1$ time step using known poses as follows:

$$\mathbf{P}_{\tau \rightarrow t+1} = \mathbf{T}_{\tau,t+1} \mathbf{P}_\tau, \quad \forall \tau \neq t+1, \quad (3)$$

where $\mathbf{T}_{\tau,t+1}$ is the transformation matrix from time step τ to $t+1$.

Previous methods then convert these continuous point clouds into discrete 2D Bird's Eye View representations. However, this process compresses the Z-axis dimension, leading to a loss of crucial spatial information. To overcome this limitation, we employ 3D voxelization to retain critical spatial information along the Z-axis. First, we divide the 3D point cloud into a 3D grid and then extract intra-voxel features using a lightweight Voxel Feature Encoder (VFE). Following [12], for each point cloud $\mathbf{P}_\tau \in \mathbb{R}^{N_\tau \times 3}$, we concatenate the 3D coordinates of each point cloud (x, y, z) , the offsets from voxel center $(x - x_v, y - y_v, z - z_v)$, and the offsets from cluster center

$(x - x_c, y - y_c, z - z_c)$ to form a tensor of shape $\mathbb{R}^{N_\tau \times 9}$. By applying linear layers followed by Batch Normalization and ReLU, we obtain the initial point-wise features $\mathbf{f}_\tau^p \in \mathbb{R}^{N_\tau \times 16}$. The initial voxel features $\mathbf{f}_\tau^v \in \mathbb{R}^{W \times L \times H \times 16}$ are obtained by performing voxel-wise average pooling on the \mathbf{f}_τ^p . We expand \mathbf{f}_τ^v by adding a time step dimension, resulting in a tensor of shape $\mathbb{R}^{W \times L \times H \times 1 \times 16}$. Then, by concatenating these tensors, which are derived from five consecutive frames, along the time step axis, we obtain $\mathbf{f}^4D \in \mathbb{R}^{W \times L \times H \times 5 \times 16}$. Thanks to this early fusion strategy, where fusion is performed right after the VFE for each point cloud, our method can effectively utilize a larger number of frames.

C. 4D Voxel Scene Flow Network

To directly extract spatio-temporal features, we design a 4D voxel network with an hourglass architecture incorporating skip connections. 2D convolution kernels primarily focus on spatial relationships within the height and width dimensions, implicitly extracting temporal features. In contrast, 3D and 4D convolutions, including the time dimension, directly process both spatial and temporal information at the kernel level. This allows for explicit extraction of spatio-temporal features. Although using 4D convolutions ensures high performance, it also incurs significant computational overhead. To address this issue, we propose the Spatio-Temporal Decomposition Block (STDB), which achieves similar performance to 4D convolution while operating more efficiently. We replace the 4D convolution layer with a kernel size of $3 \times 3 \times 3 \times 3$ with a combination of a spatial convolution layer of $3 \times 3 \times 3 \times 1$ and a temporal convolution layer of $1 \times 1 \times 1 \times 3$. These

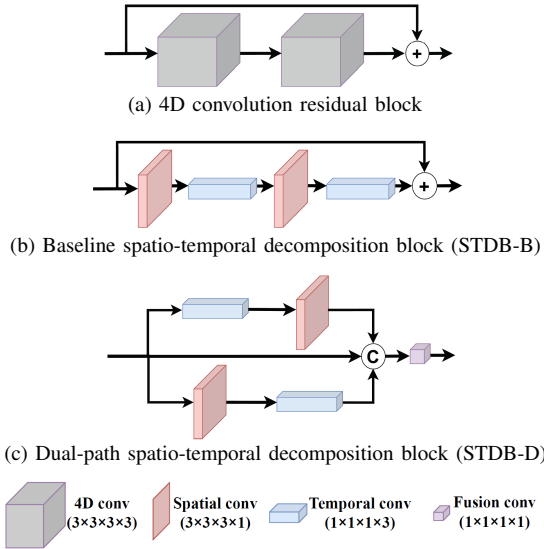


Fig. 3. Comparison of spatio-temporal feature extraction blocks.

layers operate on the 4D voxel as 3D and 1D convolutions, respectively, allowing for reduced memory usage and increased computational speed compared to the baseline using 4D convolution. We introduce two types of decomposition blocks to replace the 4D convolution residual block.

Parallel Spatio-Temporal Decomposition Block: First, we propose a parallel decomposition approach, where a 3D spatial convolution and a 1D temporal convolution are applied in parallel, as shown in Fig. 2. The 3D spatial convolution captures spatial features, while the 1D temporal convolution processes the time step dimension, focusing on temporal cues. Their outputs are fused using a 1D convolution, combining spatial and temporal features into a unified representation. This parallel approach efficiently extracts and integrates spatial and temporal features, reducing computational overhead.

Dual-path Spatio-Temporal Decomposition Block: Secondly, we present a dual-path decomposition approach, as seen in Fig. 3-(c). In the top branch, a 3D spatial convolution is followed by a 1D temporal convolution. Conversely, in the bottom branch, a 1D temporal convolution is followed by a 3D spatial convolution. The outputs from these two branches are then fused using a 1D convolution. This dual-path decomposition block extracts spatial and temporal features in different sequences before combining them, enhancing the efficiency and flexibility of feature extraction.

We design the 4D voxel network by applying the Spatio-Temporal Decomposition Block (STDB) twice at each level of the encoder and once at each level of the decoder. We utilize submanifold sparse convolution [20] for all 1D, 3D, and 4D convolutions to enhance computational efficiency. The details of the network are provided in Table I.

D. Point Head

Since the 4D voxel network outputs only inter-voxel features, we use a simple point head to output point-wise scene flow vector at the current time step t . First, we extract the features at the current time step t from the output 5D tensor $\hat{\mathbf{f}}^{4D}$ \in

TABLE I

DETAILS OF 4D VOXEL NETWORK. EACH STDB-P CONSISTS OF TWO SETS OF CONVOLUTION LAYERS (SPATIAL, TEMPORAL, AND FUSION CONV). THE VALUES (X, Y) IN THE STDB-P COLUMN REPRESENT THE NUMBER OF FILTERS FOR EACH OF THESE SETS. EACH STAGE PERFORMS POOLING OR UPSAMPLING AFTER THE STDB-P.

Stage	STDB-P (Filters)	Pool & Up (Kernel, Stride)	Output shape [W \times L \times H \times T \times ch]
Input			512 \times 512 \times 32 \times 5 \times 16
Encoder	1 (16, 32) (32, 32)	Pool (2,2,2,1)	256 \times 256 \times 16 \times 5 \times 32
	2 (32, 64) (64, 64)	Pool (2,2,2,1)	128 \times 128 \times 8 \times 5 \times 64
	3 (64, 64) (64, 64)	Pool (2,2,2,1)	64 \times 64 \times 4 \times 5 \times 64
	4 (64, 64) (64, 64)	Pool (2,2,1,1)	32 \times 32 \times 4 \times 5 \times 64
	5 (64, 64) (64, 64)	Up (2,2,1,1)	32 \times 32 \times 4 \times 5 \times 64
Decoder	6 (64, 64)	Up (2,2,2,1)	64 \times 64 \times 4 \times 5 \times 64
	7 (64, 64)	Up (2,2,2,1)	128 \times 128 \times 8 \times 5 \times 64
	8 (64, 64)	Up (2,2,2,1)	256 \times 256 \times 16 \times 5 \times 64
	9 (32, 16)	-	512 \times 512 \times 32 \times 5 \times 16

$\mathbb{R}^{W \times L \times H \times 5 \times 16}$, which is the output of the 4D voxel network, and then squeeze the time step dimension to form a 4D tensor $\hat{\mathbf{f}}_t^v \in \mathbb{R}^{W \times L \times H \times 16}$. Then, we convert these voxel-wise features $\hat{\mathbf{f}}_t^v$ into point-wise features $\hat{\mathbf{f}}_t^{v \rightarrow p} \in \mathbb{R}^{N_t \times 16}$. We concatenate $\hat{\mathbf{f}}_t^{v \rightarrow p}$ with the initial point-wise features \mathbf{f}_t^p generated through voxel feature encoder. Finally, we utilize two MLP layers to output the point-wise motion vectors $\hat{\mathbf{F}}_{t,t+1}^{\text{motion}} \in \mathbb{R}^{N_t \times 3}$.

IV. EXPERIMENTS

In this section, we demonstrate the superiority of the proposed Flow4D in the scene flow task. In Section IV-A, we describe the dataset, metrics, and training details used in the experiments. Then, we quantitatively and qualitatively compare the proposed method with other state-of-the-art methods in Section IV-B. In Section IV-C, we validate the effectiveness of each module of Flow4D through ablation studies. Finally, analysis of the computational time is discussed in Section IV-D.

A. Experimental Settings

Dataset: We utilize the large-scale Argoverse 2 dataset [11] to evaluate the proposed method. The Argoverse 2 dataset comprises 110,071 training data and 23,573 test data. Ground truth is not provided for the test set, and the evaluation for the test set is conducted on the official benchmark server. Since Argoverse 2 is the only LiDAR-based scene flow dataset with a blind test server, we focus experiments on the Argoverse 2.

Metrics: The Argoverse 2 2024 scene flow challenge uses Bucket Normalized Endpoint Error (EPE) [10] as the main metric, while the Argoverse 2 2023 scene flow challenge used Three-way EPE [33] as the main metric. Following this, we use the Bucket Normalized EPE and the Three-way EPE as main metrics. Due to the severe class imbalance in LiDAR point clouds, simply using average EPE tends to focus on the EPE of static objects. To address this, Three-way EPE calculates the EPE for dynamic foreground (FD), static foreground (FS), and static background (BS) separately and then averages them.

TABLE II

QUANTITATIVE COMPARISON ON THE ARGOVERSE 2 TEST SET. ‘SUP.’ INDICATES SUPERVISED METHODS AND ‘# F.’ REPRESENTS THE NUMBER OF INPUT FRAMES. ‘FD’ REPRESENTS FOREGROUND DYNAMIC, ‘BS’ REPRESENTS BACKGROUND STATIC, AND ‘FS’ REPRESENTS FOREGROUND STATIC.

Method	Sup.	# F.	Bucketed Normalized Endpoint Error (↓)						3-way Endpoint Error (↓)			
			Dynamic				Static	3-way Endpoint Error (↓)				
			mean	Car	Other vehicles	Pedestrian		mean	Avg.	FD	BS	FS
ZeroFlow 1x [8]		2	0.5941	0.3267	0.4756	0.9663	0.6078	0.0195	-	-	-	-
ZeroFlow XL 5x [8]		2	0.4389	0.2382	0.2577	0.7225	0.4517	0.0143	0.0510	0.1239	0.0106	0.0184
NSFP [5]		2	0.4219	0.2509	0.3313	0.7225	0.3831	0.0279	0.0606	0.1158	0.0344	0.0316
Liu et al. [7]		2	0.4134	0.3095	0.5586	0.5092	0.2761	0.0855	0.1307	0.1900	0.1064	0.0956
FastNSF [6]		2	0.3826	0.2961	0.4126	0.5002	0.3215	0.0736	0.1118	0.1634	0.0907	0.0814
ICP-Flow [9]		2	0.3309	0.1945	0.3314	0.4353	0.3626	0.0271	0.0650	0.1369	0.0250	0.0332
SeFlow [25]		2	0.3194	0.2178	0.3464	0.4452	0.2683	0.0148	0.0536	0.1323	0.0043	0.0242
FastFlow3D [3]	✓	2	0.5323	0.2429	0.3908	0.9818	0.5139	0.0182	0.0735	0.1917	0.0027	0.0262
DeFlow [4]	✓	2	0.3704	0.1530	0.3150	0.6615	0.3520	0.0262	0.0501	0.1091	0.0062	0.0352
TrackFlow [10]	✓	2	0.2689	0.1817	0.3054	0.3581	0.2302	0.0447	0.0473	0.1030	0.0024	0.0365
Ours	✓	2	<u>0.1738</u>	<u>0.0954</u>	<u>0.1671</u>	<u>0.2775</u>	<u>0.1554</u>	<u>0.0123</u>	<u>0.0251</u>	<u>0.0573</u>	<u>0.0030</u>	<u>0.0148</u>
Ours	✓	5	0.1454	0.0871	0.1505	0.2165	0.1272	0.0106	0.0224	0.0494	0.0047	0.0130

TABLE III
QUANTITATIVE COMPARISON ON THE ARGOVERSE 2 VALIDATION SET.

Method	# Frames	Bucketed Normalized EPE (↓)			3-way Endpoint Error (↓)				Dynamic IoU (↑)	
		mean	Dynamic	mean	Static	Avg.	FD	BS		
FastFlow3D [3]	2	0.6245		0.0146		0.0852	0.2326	<u>0.0025</u>	0.0206	<u>0.5257</u>
DeFlow [4]	2	0.4305		0.0207		0.0516	0.1212	0.0047	0.0289	<u>0.5227</u>
Ours	2	0.2047		0.0121		0.0318	0.0773	0.0024	0.0157	0.6909
Ours	5	0.1641		0.0104		0.0283	0.0675	0.0039	0.0134	<u>0.6278</u>

TABLE IV
COMPARISON OF THE PROPOSED SPATIO-TEMPORAL DECOMPOSITION BLOCKS.

Module	Bucketed Normalized EPE (↓)		GFLOPs
	Mean Dynamic	Mean Static	
4D conv	<u>0.1662</u>	0.0097	152.0
STDB-B	0.1901	0.0115	58.6
STDB-D	0.1719	0.0108	65.1
STDB-P	0.1641	<u>0.0104</u>	67.8

TABLE VI
PERFORMANCE COMPARISON OF DIFFERENT COMPONENT CONFIGURATIONS. ‘T. F.’ DENOTES TEMPORAL FUSION AND ‘B. N. EPE’ DENOTES BUCKETED NORMALIZED EPE.

Method	Components				B. N. EPE (↓)	
	P / V	T. F.	# Frames	STDB-P	mean D.	mean S.
DeFlow	Pillar		2		0.4305	0.0207
(a)	Pillar	✓	2		0.2447	0.0127
(b)	Voxel	✓	2		0.2084	0.0113
(c)	Voxel	✓	5		<u>0.1662</u>	0.0097
Flow4D	Voxel	✓	5	✓	0.1641	<u>0.0104</u>

TABLE V
PERFORMANCE AND COMPUTATIONAL EFFICIENCY BASED ON THE NUMBER OF INPUT FRAMES.

# Frames	Bucketed Normalized EPE (↓)		Efficiency
	Mean Dynamic	Mean Static	
2	0.2047	0.0121	1.48 18.9
3	0.1812	0.0109	1.53 17.8
4	<u>0.1712</u>	<u>0.0101</u>	1.57 16.4
5	0.1641	0.0104	1.62 15.1
10	0.1728	0.0090	2.00 10.9

TABLE VII
COMPUTATION TIME FOR EACH STAGE OF THE FLOW4D.

Stage	Warping	Voxelization	4D Network	Head	Total
[ms]	0.8	18.4	46.4	0.6	66.2

B. Comparison

We compare the proposed method with various supervised and self-supervised LiDAR scene flow methods. Table II shows the comparison results evaluated through the official test server of Argoverse 2. The proposed method achieves a mean Dynamic Normalized EPE of 0.1454, which is 45.9% better than the state-of-the-art method, TrackFlow [10], and 60.7% better than DeFlow [4], demonstrating remarkable performance. Additionally, the proposed method outperforms all existing methods in class-specific Dynamic Normalized EPE and mean Static Normalized EPE. Even when using only 2 frames, the proposed method surpasses TrackFlow by 35.4% in mean Dynamic Normalized EPE. Additionally, as shown in Table III, we further compare the proposed method with supervised methods FastFlow3D [3] and DeFlow [4] on the

Furthermore, Bucket Normalized EPE divides classes into background, car, other-vehicle, pedestrian, and wheeled-VRU, and normalizes errors based on the speed of the objects, enabling a more detailed and accurate performance comparison.

Training Details: We train the model using the DeFlow loss [4], which effectively scales dynamic and static points, with the Adam optimizer ($lr=1e-3$) for 15 epochs. In the voxelization process, each voxel size is [20cm, 20cm, 20cm], and the voxelization range is [51.2m, 51.2m, 6.4m]. Finally, the resolution of the 4D voxel space is $[W = 512, L = 512, H = 32, T = 5]$.

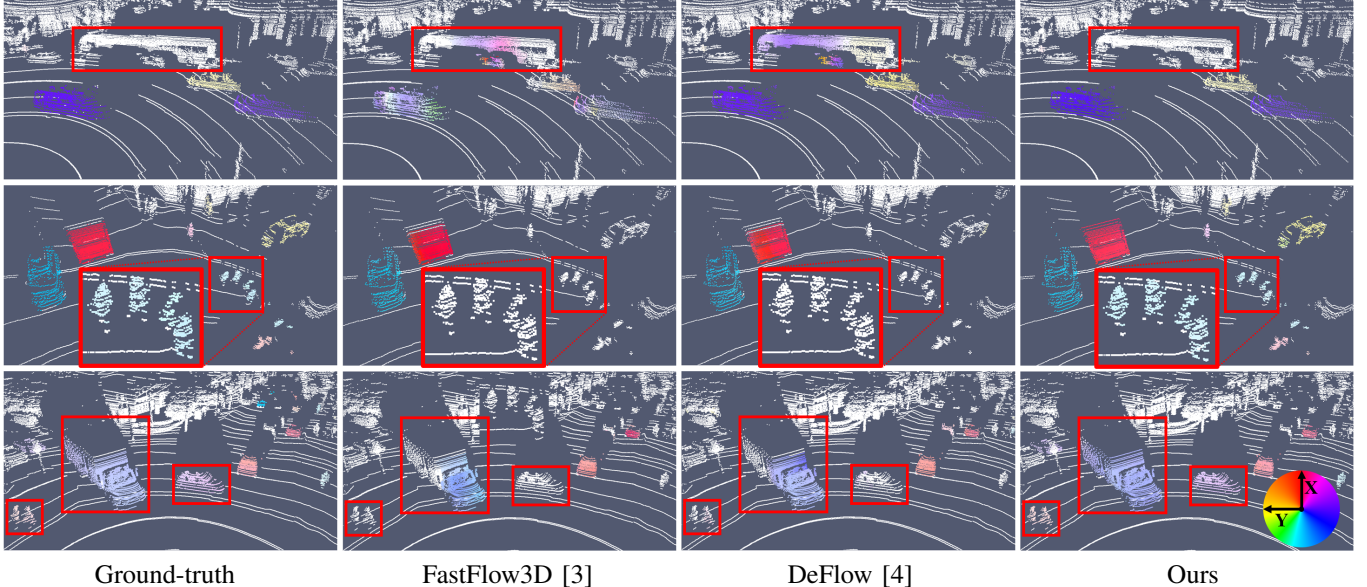


Fig. 4. Qualitative comparison on Argoverse 2 validation set. Following DeFlow [4], we represent the direction and magnitude of each motion vector as hue and saturation, respectively. Our proposed method estimates motion vectors more accurately than existing methods [3], [4] for all classes, including pedestrians, vehicles, trucks, and buses.

Argoverse 2 validation set. We define dynamic points using a 0.5 m/s threshold and compare the Dynamic IoU. When using 2 frames, our method achieves a 52.5% lower mean Dynamic Normalized EPE compared to DeFlow. Furthermore, using 5 frames results in an additional 19.8% performance improvement over using 2 frames. These results demonstrate the superiority of the proposed Flow4D. Additionally, we present qualitative comparisons in Fig. 4. As shown in Fig. 4, Flow4D performs more accurate motion vectors for all classes compared to FastFlow3D [3] and DeFlow [4]. For more detailed results, please refer to the multimedia attachment.

C. Ablation Studies

To provide a comprehensive analysis of the contributions of each element, we conduct further experiments to evaluate the proposed Spatio-Temporal Decomposition Blocks (STDB), the impact of varying the number of input frames, and the effectiveness of each component on the Argoverse 2 validation set.

Spatio-Temporal Decomposition Block: Table IV shows the performance comparison between the 4D convolution residual block (Fig. 3a), the Baseline STDB (Fig. 3b), the Dual-path STDB (Fig. 3c), and the Parallel STDB (Fig. 2). The STDB-Baseline requires 61.4% less GFLOPs compared to using the 4D convolution, but suffers a 14.4% increase in mean Dynamic EPE. The STDB-Dual-path consumes 11.1% more GFLOPs compared to the STDB-B but achieves a 9.6% reduction in mean Dynamic EPE. Lastly, the STDB-Parallel has a 16.6% higher computational load compared to the STDB-B, but shows a 55.4% lower computational load compared to using the 4D Conv while achieving superior mean Dynamic EPE.

Number of frames: We analyze the performance and efficiency based on the number of frames used, as shown in Table V. Increasing the number of frames tends to improve performance,

but also increases the computational overhead. The proposed method outperforms the current state-of-the-art even with just two frames, making it advisable to use two frames in scenarios where efficiency is a priority. When using five frames, Flow4D achieves the lowest mean Dynamic EPE, and when using ten frames, it achieves the lowest mean Static EPE. Thanks to the early-fusion strategy, the proposed method does not experience a significant increase in computational overhead with more frames, and it can operate in real-time using only 1.62GiB of GPU memory when using five frames. Considering both performance and efficiency, we employ five frames as the default setting for the proposed Flow4D.

Effectiveness of each component: Table VI shows the effectiveness of each component of the proposed method. DeFlow [4] converts two point clouds into 2D BEV and applies individual 2D encoders. Method (a) retains the pillar-based representation but stacks the 2D BEV features $[W, L, 16]$, obtained from the pillar feature encoder, along the time axis to create a 4D tensor $[W, L, 2, 16]$. Then, it utilizes the 3D voxel network, reducing the mean Dynamic EPE to 0.2447 ($\downarrow 43.2\%$). Method (b) transitions from pillar-based to a voxel-based representation, resulting in a mean Dynamic EPE of 0.2084 ($\downarrow 14.8\%$ compared to (a)). Increasing the number of input frames from 2 to 5 (method (c)) results in an additional 20.2% performance improvement. Finally, the application of the Spatio-Temporal Decomposition Block (STDB) results in an additional 1.3% performance improvement. Incorporating all these components, the proposed Flow4D shows a 61.9% performance improvement over DeFlow [4].

D. Computational Time

Table VII shows the computation time required for each component of Flow4D. The proposed method takes a total of 66.2 ms from point cloud warping to output on the

NVIDIA RTX 3090. Among the total computation time, the 4D voxel network takes 46.4 ms, and the voxelization process takes 18.4 ms. The proposed Flow4D processes each of the five input frames through 3D voxelization, contributing some computational overhead during the voxelization stage. Nevertheless, the proposed method operates at 15.1 FPS, making real-time operation feasible in autonomous driving systems.

V. CONCLUSION

In this paper, we propose Flow4D, a novel 4D voxel-based LiDAR scene flow framework. The proposed method takes five 3D point clouds and converts them into 3D voxels using an intra-voxel feature encoder (VFE). Then, it expands the dimension of each 3D voxel by adding a time dimension and concatenates them along this axis to create a 4D voxel. Through the 4D voxel network, it explicitly extracts spatial and temporal information simultaneously. To reduce the heavy computational load of 4D convolution, we introduce the Spatio-Temporal Decomposition Block (STDB), which decomposes 4D convolution into 3D spatial convolution and 1D temporal convolution. Furthermore, Flow4D is designed with an early fusion scheme that fuses features immediately after the VFE, allowing it to effectively exploit more temporal cues from a larger number of point clouds. These contributions enable our method to achieve a significant performance improvement of 45.9% over the previous state-of-the-art while being efficient enough to run in real-time on a desktop GPU. In the future, we plan to develop an even more efficient framework capable of real-time operation on embedded systems.

REFERENCES

- [1] J. Li, C. Luo, and X. Yang, “Pillarnext: Rethinking network designs for 3d object detection in lidar point clouds,” in *Proceedings of IEEE Conference on Computer Vision and Pattern Recognition (CVPR)*, 2023, pp. 17 567–17 576.
- [2] Y. Liu, L. Kong, X. Wu, R. Chen, X. Li, L. Pan, Z. Liu, and Y. Ma, “Multi-space alignments towards universal lidar segmentation,” in *Proceedings of IEEE Conference on Computer Vision and Pattern Recognition (CVPR)*, 2024, pp. 14 648–14 661.
- [3] P. Jund, C. Sweeney, N. Abdo, Z. Chen, and J. Shlens, “Scalable scene flow from point clouds in the real world,” *IEEE Robotics and Automation Letters*, vol. 7, no. 2, pp. 1589–1596, 2022.
- [4] Q. Zhang, Y. Yang, H. Fang, R. Geng, and P. Jensfelt, “Deflow: Decoder of scene flow network in autonomous driving,” in *Proceedings of IEEE International Conference on Robotics and Automation (ICRA)*. IEEE, 2024.
- [5] X. Li, J. Kaesemeyer Pontes, and S. Lucey, “Neural scene flow prior,” *Advances in Neural Information Processing Systems*, vol. 34, pp. 7838–7851, 2021.
- [6] X. Li, J. Zheng, F. Ferroni, J. K. Pontes, and S. Lucey, “Fast neural scene flow,” in *Proceedings of IEEE International Conference on Computer Vision (ICCV)*, 2023, pp. 9878–9890.
- [7] D. Liu, D. Liu, X. Li, S. Lin, B. Wang, X. Chang, L. Chu, et al., “Self-supervised multi-frame neural scene flow,” *arXiv preprint arXiv:2403.16116*, 2024.
- [8] K. Vedder, N. Peri, N. E. Chodosh, I. Khatri, E. Eaton, D. Jayaraman, Y. Liu, D. Ramanan, and J. Hays, “Zeroflow: Scalable scene flow via distillation,” in *International Conference on Learning Representations (ICLR)*, 2024.
- [9] Y. Lin and H. Caesar, “Icp-flow: Lidar scene flow estimation with icp,” in *Proceedings of IEEE Conference on Computer Vision and Pattern Recognition (CVPR)*, 2024.
- [10] I. Khatri, K. Vedder, N. Peri, D. Ramanan, and J. Hays, “I can’t believe it’s not scene flow!” *arXiv preprint arXiv:2403.04739*, 2024.
- [11] B. Wilson, W. Qi, T. Agarwal, J. Lambert, J. Singh, S. Khandelwal, B. Pan, R. Kumar, A. Hartnett, J. K. Pontes, D. Ramanan, P. Carr, and J. Hays, “Argoverse 2: Next generation datasets for self-driving perception and forecasting,” in *Proceedings of the Neural Information Processing Systems Track on Datasets and Benchmarks (NeurIPS Datasets and Benchmarks 2021)*, 2021.
- [12] A. H. Lang, S. Vora, H. Caesar, L. Zhou, J. Yang, and O. Beijbom, “Pointpillars: Fast encoders for object detection from point clouds,” in *Proceedings of IEEE Conference on Computer Vision and Pattern Recognition (CVPR)*, 2019, pp. 12 697–12 705.
- [13] T. Cortinhal, G. Tzelepis, and E. Erdal Aksoy, “Salsanext: Fast, uncertainty-aware semantic segmentation of lidar point clouds,” in *Advances in Visual Computing: 15th International Symposium, ISVC 2020, San Diego, CA, USA, October 5–7, 2020, Proceedings, Part II 15*. Springer, 2020, pp. 207–222.
- [14] A. Ando, S. Gidaris, A. Bursuc, G. Puy, A. Boulch, and R. Marlet, “Rangevit: Towards vision transformers for 3d semantic segmentation in autonomous driving,” in *Proceedings of IEEE Conference on Computer Vision and Pattern Recognition (CVPR)*, 2023, pp. 5240–5250.
- [15] H. Thomas, C. R. Qi, J.-E. Deschaud, B. Marcotegui, F. Goulette, and L. J. Guibas, “Kpconv: Flexible and deformable convolution for point clouds,” in *Proceedings of IEEE International Conference on Computer Vision (ICCV)*, 2019, pp. 6411–6420.
- [16] Q. Hu, B. Yang, L. Xie, S. Rosa, Y. Guo, Z. Wang, N. Trigoni, and A. Markham, “Randla-net: Efficient semantic segmentation of large-scale point clouds,” in *Proceedings of IEEE Conference on Computer Vision and Pattern Recognition (CVPR)*, 2020, pp. 11 108–11 117.
- [17] C. Choy, J. Gwak, and S. Savarese, “4d spatio-temporal convnets: Minkowski convolutional neural networks,” in *Proceedings of IEEE Conference on Computer Vision and Pattern Recognition (CVPR)*, 2019, pp. 3075–3084.
- [18] X. Zhu, H. Zhou, T. Wang, F. Hong, Y. Ma, W. Li, H. Li, and D. Lin, “Cylindrical and asymmetrical 3d convolution networks for lidar segmentation,” in *Proceedings of IEEE Conference on Computer Vision and Pattern Recognition (CVPR)*, 2021, pp. 9939–9948.
- [19] B. Liu, M. Wang, H. Foroosh, M. Tapen, and M. Pensky, “Sparse convolutional neural networks,” in *Proceedings of IEEE Conference on Computer Vision and Pattern Recognition (CVPR)*, 2015, pp. 806–814.
- [20] B. Graham and L. Van der Maaten, “Submanifold sparse convolutional networks,” *arXiv preprint arXiv:1706.01307*, 2017.
- [21] H. Mittal, B. Okorn, and D. Held, “Just go with the flow: Self-supervised scene flow estimation,” in *Proceedings of the IEEE/CVF conference on computer vision and pattern recognition*, 2020, pp. 11 177–11 185.
- [22] J. K. Pontes, J. Hays, and S. Lucey, “Scene flow from point clouds with or without learning,” in *2020 international conference on 3D vision (3DV)*. IEEE, 2020, pp. 261–270.
- [23] Y. Kittenplon, Y. C. Eldar, and D. Raviv, “Flowstep3d: Model unrolling for self-supervised scene flow estimation,” in *Proceedings of the IEEE/CVF Conference on Computer Vision and Pattern Recognition*, 2021, pp. 4114–4123.
- [24] R. Li, C. Zhang, G. Lin, Z. Wang, and C. Shen, “Rigidflow: Self-supervised scene flow learning on point clouds by local rigidity prior,” in *Proceedings of IEEE Conference on Computer Vision and Pattern Recognition (CVPR)*, 2022, pp. 16 959–16 968.
- [25] Q. Zhang, Y. Yang, P. Li, O. Andersson, and P. Jensfelt, “Seflow: A self-supervised scene flow method in autonomous driving,” *arXiv preprint arXiv:2407.01702*, 2024.
- [26] A. Behl, D. Paschalidou, S. Donné, and A. Geiger, “Pointflownet: Learning representations for rigid motion estimation from point clouds,” in *Proceedings of the IEEE/CVF Conference on Computer Vision and Pattern Recognition*, 2019, pp. 7962–7971.
- [27] X. Liu, C. R. Qi, and L. J. Guibas, “Flownet3d: Learning scene flow in 3d point clouds,” in *Proceedings of the IEEE/CVF conference on computer vision and pattern recognition*, 2019, pp. 529–537.
- [28] G. Puy, A. Boulch, and R. Marlet, “Flot: Scene flow on point clouds guided by optimal transport,” in *European conference on computer vision*. Springer, 2020, pp. 527–544.
- [29] W. Wu, Z. Y. Wang, Z. Li, W. Liu, and L. Fuxin, “Pointpwc-net: Cost volume on point clouds for (self-) supervised scene flow estimation,” in *Computer Vision–ECCV 2020: 16th European Conference, Glasgow, UK, August 23–28, 2020, Proceedings, Part V 16*. Springer, 2020, pp. 88–107.
- [30] K.-H. Lee, M. Kliemann, A. Gaidon, J. Li, C. Fang, S. Pillai, and W. Burgard, “Pillarflow: End-to-end birds-eye-view flow estimation for autonomous driving,” in *2020 IEEE/RSJ International Conference on Intelligent Robots and Systems (IROS)*. IEEE, 2020, pp. 2007–2013.

- [31] R. Li, G. Lin, T. He, F. Liu, and C. Shen, “Hcrf-flow: Scene flow from point clouds with continuous high-order crfs and position-aware flow embedding,” in *Proceedings of the IEEE/CVF Conference on Computer Vision and Pattern Recognition*, 2021, pp. 364–373.
- [32] R. Battrawy, R. Schuster, M.-A. N. Mahani, and D. Stricker, “Rms-flownet: Efficient and robust multi-scale scene flow estimation for large-scale point clouds,” in *Proceedings of IEEE International Conference on Robotics and Automation (ICRA)*. IEEE, 2022.
- [33] N. Chodosh, D. Ramanan, and S. Lucey, “Re-evaluating lidar scene flow for autonomous driving,” in *Proceedings of IEEE Winter Conference on Applications of Computer Vision (WACV)*, 2023.